Supplementary material 'Phase diagram and effective shape of semi-flexible colloidal rods and biopolymers'

M. Dennison,[1] M. Dijkstra,[1] and R. van Roij[2]

[1] *Soft Condensed Matter, Debye Institute for Nanomaterials Science, Utrecht University, Princetonplein 5, 3584 CC Utrecht, The Netherlands*

[2] *Institute for Theoretical Physics, Utrecht University, Leuvenlaan 4, 3584 CE Utrecht, The Netherlands*

(Dated: April 7, 2011)

In this supplementary material, we give a full description of the model of binary systems of semi-flexible rods, using an Onsager-type second-virial approach for a segmented-chain model. We also present results for the convergence of the equation of state for fd virus particles, and the properties of fd virus particles of various flexibilities. Finally, we compare our predicted phase diagrams for binary fd virus mixtures with those obtained experimentally.

I. THEORY

A. Free-energy minimization and phase diagrams

In the Onsager theory of nematic liquid crystals [1], the isotropic-nematic (I-N) phase transition of a one-component system of rigid rods is driven by competition between two entropies. One is similar to entropy of mixing, arising from the mixing of particles of different orientations. The other arises from the excluded volume interactions of the particles. These are expressed via the Helmholtz free energy, F, and for monodisperse rigid particles the solutions to this are well known (see e.g. [2, 3]). Extending the theory to mixtures requires the addition of an extra mixing term to the Helmholtz free energy [4, 5]. Flexibility may be incorporated in numerous ways (see e.g. [6–10]), and in this supplementary material, we build on the work of Wessels and Mulder [6] to describe binary systems of semi-flexible rods.

We consider a suspension of N_i semi-flexible rods of species $i = 1, 2$ with contour lengths L_i, in a volume V at temperature T. Following Wessels and Mulder [6] we model a rod of species i as a chain of M_i rod-like segments of length $l_i = L_i/M_i$ and diameter $D_i \ll l_i$. Denoting the orientation of the m-th segment by a unit-vector ω_m (with $1 \leq m \leq M_i$), we write the bending energy of a chain of species i with orientation $\mathbf{\Omega} = \{\omega_1, \ldots, \omega_{M_i}\}$ as

$$U_i(\mathbf{\Omega}) = \sum_{m=1}^{M_i-1} u_i(\omega_m, \omega_{m+1}) = -\frac{P_i}{l_i} \sum_{m=1}^{M_i-1} \omega_m \cdot \omega_{m+1}, \tag{1}$$

where the stiffness is described in terms of the persistence length P_i [6]. Here and below we use thermal energy units by setting $k_B T = 1$. The state of the suspension is characterized by the orientation distributions functions (ODFs) $f_i(\mathbf{\Omega})$, which satisfy the normalization condition $\int d\mathbf{\Omega} f_i(\mathbf{\Omega}) = 1$ where $d\mathbf{\Omega} = \prod_{m=1}^{M_i} d\omega_m$. Denoting the total number of rods by $N = N_1 + N_2$, the density by $\rho = N/V$, and the mole fraction of species i by $x_i = N_i/N$, we can write the variational free-energy functional $F[f_1, f_2]$ of this system within an Onsager-like second virial approximation as

$$\begin{aligned} \frac{F[f_1, f_2]}{N} &= \ln(B\rho) - 1 + x_1 \ln x_1 + x_2 \ln x_2 \\ &+ \sum_{i=1}^{2} x_i \int f_i(\mathbf{\Omega}) \Big(\ln(4\pi f_i(\mathbf{\Omega})) + U_i(\mathbf{\Omega}) \Big) d\mathbf{\Omega} \\ &+ \frac{\rho}{2} \sum_{i,j=1}^{2} x_i x_j \int f_i(\mathbf{\Omega}) f_j(\mathbf{\Omega}') K_{ij}(\mathbf{\Omega}, \mathbf{\Omega}') d\mathbf{\Omega} d\mathbf{\Omega}'. \end{aligned} \tag{2}$$

The first line of Eq. (2) represents the translational and the mixing ideal-gas contributions (with $B = \frac{\pi}{4} D_1 L_1^2$, a constant), the second line denotes the orientation entropy and bending energy, and the third line the excluded volume interactions given by

$$K_{ij}(\mathbf{\Omega},\mathbf{\Omega}') = \sum_{m=1}^{M_i}\sum_{m'=1}^{M_j} k_{ij}(\omega_m,\omega_{m'}) \\ = l_i l_j (D_i+D_j)\sum_{m=1}^{M_i}\sum_{m'=1}^{M_j} |\sin\gamma(\omega_m,\omega_{m'})|, \tag{3}$$

with $\gamma(\omega_m,\omega_{m'}) = \arccos(\omega_m\cdot\omega_{m'})$ the angle between chain segments [6] m and m'. The free-energy functional of Eq. (2) is a two-component generalization of the one-component segmented-chain functional of Ref.[6], and for $M_i = 1$ and $U_i \equiv 0$ it reduces to the Onsager functional for binary mixtures of rigid rods [4, 11].

At a given thermodynamic state point, the equilibrium ODFs minimize F and therefore satisfy the Euler-Lagrange equations $\delta(F-\mu_i N_i)/\delta f_i(\mathbf{\Omega}) = 0$ for $i = 1, 2$, with μ_i the chemical potential-like Lagrange multiplier that ensures a proper normalization. This gives rise to

$$f_i(\mathbf{\Omega}) = \frac{\exp(-U_i(\mathbf{\Omega}) - V_i(\mathbf{\Omega}))}{Q_i}; \tag{4}$$

$$V_i(\mathbf{\Omega}) = \rho\sum_{j=1}^{2} x_j \int K_{ij}(\mathbf{\Omega},\mathbf{\Omega}') f_j(\mathbf{\Omega}')d\mathbf{\Omega}', \tag{5}$$

where $V_i(\mathbf{\Omega})$ can be seen as a self-consistent field acting on all segments of a chain, and Q_i is a partition function-like normalization factor. Explicitly solving Eqs. (4) and (5) for state points of interest would be prohibitively expensive computationally because of the high-dimensional angular $\mathbf{\Omega}$-grids that would be required in the case when $M_i \gg 1$. Instead, we formally evaluate the functional F of Eq. (2) in its minimum by inserting the solutions f_i of Eqs. (4) and (5) to find the equilibrium free energy

$$\frac{F_{\rm eq}}{N} = \ln(B\rho) - 1 + x_1\ln\frac{x_1}{Q_1} + x_2\ln\frac{x_2}{Q_2} - \frac{1}{2}\rho\sum_{i,j}^{2} x_i x_j \sum_{m=1}^{M_i}\sum_{m'=1}^{M_j}\int k_{ij}(\omega,\omega') f_{i,m}(\omega) f_{j,m'}(\omega')d\omega d\omega', \tag{6}$$

where $f_{i,m}(\omega)$ is the ODF of the m-th segment ($m = 1,\ldots,M_i$) of a chain of species $i = 1, 2$ defined by

$$f_{i,m}(\omega_m) = \int f_i(\mathbf{\Omega})d\omega_1\ldots d\omega_{m-1}d\omega_{m+1}\ldots d\omega_{M_i}. \tag{7}$$

Eq. (6) implies that the thermodynamics does *not* require the full solutions $f_i(\mathbf{\Omega})$ but in fact only the M_i single-segment distributions $f_{i,m}(\omega)$ and the normalization factors Q_i, for which an efficient iterative recursion scheme, that exploits the connectivity of the chain, can be set up as follows.

Eqs. (3) and (5) allow us to write $V_i(\mathbf{\Omega}) = \sum_{m=1}^{M_i} v_i(\omega_m)$ with the *same* selfconsistent field

$$v_i(\omega_m) = \rho\sum_{j=1}^{2}\sum_{m'=1}^{M_j} x_j \int k_{ij}(\omega_m,\omega_{m'}) f_{j,m'}(\omega_{m'})d\omega_{m'}, \tag{8}$$

for all segments of chains of the same species. As a consequence, Eq. (4) combined with Eq. (7) can be written as

$$f_{i,m}(\omega) = \frac{1}{Q_i} q_{i,m}(\omega)\exp[-v_i(\omega)]q_{i,M-m+1}(\omega), \tag{9}$$

with the partial-chain partition function

$$q_{i,m}(\omega_m) = \int\prod_{n=1}^{m-1}\exp[-v_i(\omega_n) - u_i(\omega_n,\omega_{n+1})]d\omega_n. \tag{10}$$

In the formulation of Eq. (9) the m-th segment ODF is seen as the statistical weight $\exp(-v_i(\omega))$ of that segment in the (selfconsistent) field $v_i(\omega)$, combined with the weights $q_{i,m}$ and $q_{i,M-m+1}$ of the two sub-chains from segment $m \pm 1$ to the two chain ends, respectively. Interestingly, the connectivity of the chain allows us to rewrite Eq. (10) as the recursion relation

$$q_{i,m}(\omega) = \int q_{i,m-1}(\omega') \exp[-v_i(\omega') - u_i(\omega', \omega)] d\omega' \tag{11}$$

such that a loop can be set up that (i) starts with a guess for $v_i(\omega)$ for $i = 1, 2$, (ii) solves for $q_{i,m}(\omega)$ for all $i = 1, 2$ and $m = 1, \dots M_i$ using Eq. (11) together with $q_{i,1}(\omega) \equiv 1$, (iii) computes $f_{i,m}(\omega)$ and the normalization factor Q_i from Eq. (9), (iv) recalculates $v_i(\omega)$ using Eq. (8) and repeats (ii)-(iv) until convergence is found. Note that this scheme *only* requires an angular grid for ω, which in the light of the azimuthal and up-down symmetry of the isotropic and nematic phases of interest here, reduces to a single grid for the polar angle $\theta \in (0, \pi/2)$. The *only* difference with Onsager-type theories for rigid-rod mixtures is the additional calculation and storage of $q_{i,m}(\omega)$ for $1 \leq m \leq M_i$ here. With the ODFs known, F_{eq} may be calculated from Eq. (6). The osmotic pressure is then calculated from $\Pi = \rho^2 \frac{\partial F_{eq}/N}{\partial \rho}$. For a binary system, phase behavior is most easily analyzed using the Gibbs free energy per particle, $\tilde{g}(x, \Pi) = \frac{F_{eq}}{N} + \frac{\Pi}{\rho}$. By fixing Π, $\tilde{g}$ may be calculated as a function of x_2 (with $x_1 = 1 - x_2$), and performing a common tangent construction allows for the prediction of coexisting phases [4, 5, 12]. For the special case of a monodisperse system, we simply set $x_2 = 0$.

We may also calculate the nematic order parameter $S_{i,m}$ of the m-th segment of a chain of species i as

$$S_{i,m} = \int d\omega f_{i,m}(\omega) P_2(\omega \cdot \mathbf{n}), \tag{12}$$

where $P_2(\omega \cdot \mathbf{n})$ is the second Legendre polynomial, and $\mathbf{n}$ is the nematic director. We define the nematic order of a rod as the average nematic order along the chain

$$S_i = \frac{1}{M_i} \sum_{m=1}^{M_i} S_{i,m}. \tag{13}$$

B. Effective length

The calculation of the effective length goes as follows. We define the mean square effective length $L_{e,i}^2$ as

$$\begin{aligned} L_{e,i}^2 &= l_i^2 \sum_{m=1}^{M_i} \sum_{m'=1}^{M_i} \langle \omega_m \cdot \omega_{m'} \rangle \\ &= l_i^2 \sum_{m=1}^{M_i} \sum_{m'=1}^{M_i} \int (\omega \cdot \omega') f_{i,m,m'}(\omega, \omega') d\omega d\omega', \end{aligned} \tag{14}$$

where we are summing the squares of the average length projections of all chain segments m' along the director of all segments m. Here, $f_{i,m,m'}(\omega, \omega')$ is the pair orientational distribution function (PDF) defined by

$$f_{i,m,m'}(\omega, \omega') = \int f_i(\mathbf{\Omega}) \delta(\omega_m - \omega) \delta(\omega_{m'} - \omega') d\mathbf{\Omega}, \tag{15}$$

where we are integrating out all other degrees of freedom from $f_i(\mathbf{\Omega})$ except those of segments m and m'. Note that $f_{i,m,m'}(\omega, \omega')$ is the probability that a chain of species i is in a configuration with the m-th and m'-th segment having orientations ω and ω', simultaneously. Inserting Eq. (4) into Eq. (15), and using Eqs. (8) and (10), we find that

$$f_{i,m,m'}(\omega, \omega') = \frac{1}{Q_i} q_{i,m}(\omega) \exp[-v_i(\omega)] Q_{i,m,m'}(\omega, \omega') \exp[-v_i(\omega')] q_{i,M-m'+1}(\omega'), \tag{16}$$

with the same notation as before. Here $Q_{i,m,m'}(\omega,\omega')$ is the partial chain partition function that takes into account the effect of the chain segments that link segment m and segment m'. For neighboring segments $m' = m+1$ we have $Q_{i,m,m'}(\omega,\omega') = \exp[-u_i(\omega,\omega')]$, and for $m' = m+2 \ldots M$, it follows the recursion relation

$$Q_{i,m,m'}(\omega,\omega') = \int d\omega'' Q_{i,m,m'-1}(\omega,\omega'') \exp[-v_i(\omega'')] \exp[-u_i(\omega'',\omega')]. \tag{17}$$

By construction, each pair orientation distribution function also obeys the normalization condition $\int f_{i,m,m'}(\omega,\omega')d\omega d\omega' = 1$. As we already know the ODFs, and hence $q_{i,m}(\omega)$ and $v_i(\omega)$, from our phase diagram calculations, the calculation of the PDFs and $L_{e,i}$ is relatively straightforward. We use $L_{e,i}$ to calculate the diameter $D_{e,i}$ required for rigid rods to have the same excluded volume as our flexible rods, at the same state point, obtaining the effective shape of the rods.

II. FD VIRUS PARAMETERS AND VALUES

In order to accurately describe semi-flexible rods, we must ensure that we are in the continuum limit. That is, we must use a sufficient number of chain segments to ensure that our results capture the physics of a continuous chain. We do this by checking the convergence of our results with increasing M_i at fixed P_i, by adapting $l_i = L_i/M_i$. We shall now examine the one-component system fd virus system, and hence we drop the subscript i. In Fig. 1, we show the isotropic (I) and nematic (N) equation of state of a one-component fd virus system, for various M values, starting from the rigid-rod limit $M = 1$. Clearly, the isotropic branch is independent of M, while the nematic branch strongly depends on M. The I-N coexistence, which is represented by the jump, shows a phase transition that shifts to higher ρ and Π upon increasing M, reaching a well-defined continuum limit in the pressure regime of interest for $M \geq 15$. Coexistence is found at $\Pi B = 29.54$.

Varying the stiffness of semi-flexible rods can have a large effect on the properties of the nematic phase at coexistence. Fig. 2 shows the equation of state for bio-engineered fd virus particles of various persistence lengths. We see that coexistence is found at much lower densities (and osmotic pressures) for stiff rods than for flexible ones, in agreement with Refs. [6–10].

We may also calculate the nematic order parameter of each chain segment in a rod from Eq. (12). Fig. 3 shows the nematic order parameter S at a distance $r \in [0, L]$ along the rod in the nematic phase at bulk coexistence for fd virus particles of various persistence lengths. We see that rigid rods are more ordered at coexistence than flexible rods, despite phase coexistence being found at a lower density. The chain segments in the middle of the rods are also found to be more ordered than the end segments, in agreement with earlier bifurcation findings in Ref. [6].

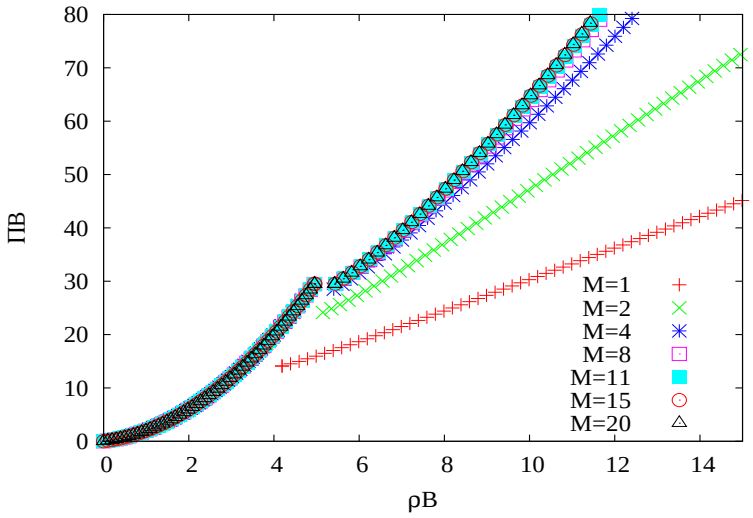

FIG. 1. Convergence of equation of state in $\rho B - \Pi B$ representation, for increasing number of chain segments M for fd virus parameters $L = 0.88\mu$m, $D = 6.6$nm and $P = 2.2\mu$m. We find that $M = 15$ is within the continuum limit for the fd virus.

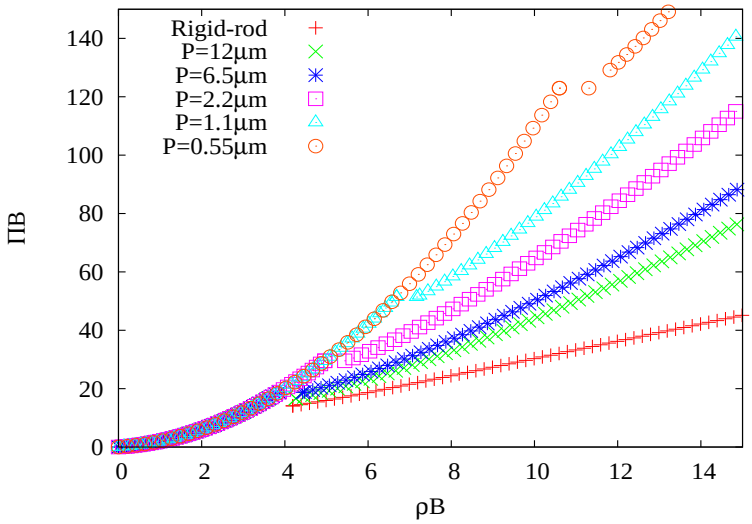

FIG. 2. Equation of state in $\rho B - \Pi B$ representation, for fd virus dimensions $L = 0.88\mu$m, $D = 6.6$nm and varying persistence length P.

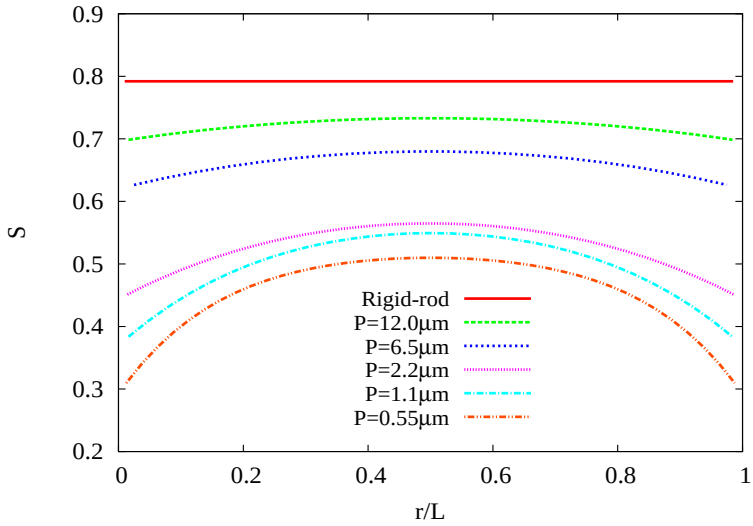

FIG. 3. Nematic order parameter S of fd virus particles of various persistence lengths in the nematic phase at bulk coexistence, at a distance $r \in [0, L]$ along the rod. The densities of the nematic phase at coexistence are: $\rho B = 4.19$, $\rho B = 4.27$, $\rho B = 4.42$, $\rho B = 5.45$, $\rho B = 7.17$ and $\rho B = 11.30$ for $P \to \infty$ (rigid-rod), $P = 12\mu$m, $P = 6.5\mu$m, $P = 2.2\mu$m, $P = 1.1\mu$m and $P = 0.55\mu$m, respectively.

III. COMPARISON TO EXPERIMENTAL DATA

In this section, we compare predicted phase diagrams for binary fd virus mixtures using both rigid and semi-flexible rods to those found experimentally in Ref. [13]. We also give details of how we convert our results from the number density ρ to concentrations in mg/ml.

Fig. 4 shows predicted phase diagrams for fd virus particles ($L_1 = L_2 = 0.88\mu$m, $D_1 = 6.6$nm and $P_1 = P_2 = 2.2\mu$m) found using rigid rods (where $M_1 = M_2 = 1$) and semi-flexible rods (with $M_1 = M_2 = 15$), and those found experimentally in Ref. [13]. In each case, we show one phase diagram where only I-N coexistence is found (low diameter ratio d), one where, in addition to I-N coexistence, N-N coexistence is observed (mid-d), and one where I-N and N-N coexistence and an I-N-N triple point are found (large d). As can be seen, at low d, both sets of theoretical predictions and the experimental results show only I-N coexistence, while at large d, each show I-N coexistence, with an N-N demixing region which begins from an I-N-N triple point. At mid-d all three show I-N and N-N demixing,

however, while both the theoretical predictions using semi-flexible rods and the experimental results show the N-N region beginning from a lower critical point, the predictions when using rigid rods show the N-N region to begin from an I-N-N triple point and ending in an upper critical point. Our results thus strongly suggest that flexibility is the key to understanding the bulk phase behavior of these systems.

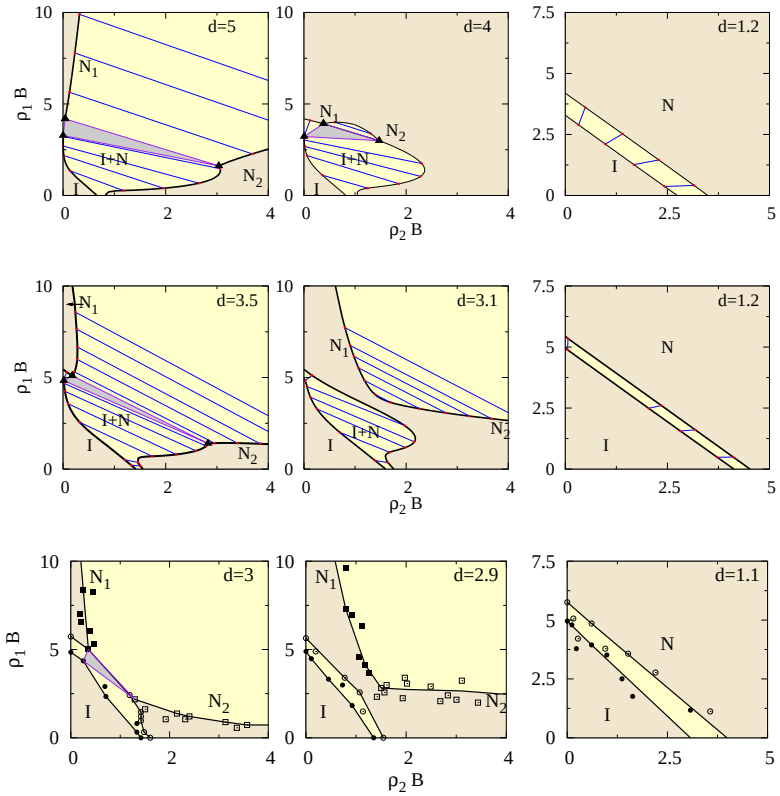

FIG. 4. Phase diagrams for mixtures of bare (thin) fd virus particles (species 1) and PEG-coated (thick) ones (species 2), with diameter various ratios (see plots). Top row shows theoretical results for rigid rods ($M_1 = M_2 = 1$), the middle row shows theoretical results for semi-flexible rods (with $M_1 = M_2 = 15$), and the bottom row shows experimental results from Ref. [13]. The lighter colored areas indicate the two-phase regions with tie-lines connecting coexisting state-points; triangles denote I-N-N and I-I-N triple points.

In order to convert between the number densities $\rho_i = N_i/V$ that we predict theoretically and the concentrations found experimentally, we use the molecular weights of the fd virus $M_{\rm fd}$ and of the polymer used as the coating, polyethylene glycol (PEG), $M_{\rm PEG}$ (given in Ref. [13] as $M_{\rm fd} = 1.64 \times 10^7$g/mol and $M_{\rm PEG} = 20000$g/mol) to calculate the mass of both the thin and thick rods (m_1 and m_2 respectively). These are given by

$$m_1 = \frac{M_{\rm fd}}{N_A}; \tag{18}$$

$$m_2 = \frac{M_{\rm fd} + N_{\rm PEG} M_{\rm PEG}}{N_A}, \tag{19}$$

where the factor $N_{\rm PEG}$ in the second line is the number of PEGs coated onto the fd virus particles (given as 200 ± 30 in Ref. [13]), and N_A is the Avogadro constant. We may then convert between the number density ρ_i and the concentration c_i in mg/ml by

$$c_i = \rho_i m_i. \tag{20}$$

In order to produce the dimensionless density $\rho_i B$, we must calculate $B = B_E = \frac{\pi}{4} D_1 L_1^2$ for the experimental systems. To take into account the electrostatic interactions of the fd virus such that it may be considered as a hard rod, Ref. [13] defines the diameter D_1 of the bare fd virus as an effective diameter D_{eff} which decreases with increasing

ionic strength [14]. We therefore calculate the scaling factor as $B_E = \frac{\pi}{4} D_{eff} L_1^2$ where $L_1 = 0.88\mu$m, the fd virus length. We may then compare our theoretical results expressed in $\rho_i B$ units against experimental results expressed in identical dimensionless units as $\rho_i B = c_i B_E / m_i$.

---

[1] L. Onsager, Ann. N.Y. Acad. Sci. **51**, 627 (1949).
[2] B. Tjipto-Margo and G. T. Evans, J. Chem. Phys. **93**, 4254 (1990).
[3] R. F. Kayser and H. J. Raveché, Phys. Rev. A **17**, 2067 (1978).
[4] R. van Roij, B. Mulder, and M. Dijkstra, Physica A **261**, 374 (1998).
[5] G. J. Vroege and H. N. W. Lekkerkerker, Rep. Prog. Phys. **55**, 1241 (1992).
[6] P. P. F. Wessels and B. M. Mulder, Soft Materials **1**, 313 (2003); J. Phys. Cond. Matt. **18**, 9335 (2006).
[7] A. R. Khokhlov and A. N. Semenov, Physica A **108**, 546 (1981); **112**, 605 (1982).
[8] Z. Y. Chen, Macromolecules **26**, 3419 (1993).
[9] M. Dijkstra and D. Frenkel, Phys. Rev. E **51**, 5891 (1995).
[10] T. Odijk, Macromolecules **19**, 2313 (1986).
[11] G. J. Vroege and H. N. W. Lekkerkerker, J. Phys. Chem. **97**, 3601 (1993).
[12] R. van Roij, Eur. J. Phys. **26**, S57 (2005).
[13] K. R. Purdy, S. Varga, A. Galindo, G. Jackson, and S. Fraden, Phys. Rev. Lett. **94**, 057801 (2005).
[14] K. R. Purdy and S. Fraden, Phys. Rev. E **70**, 061703 (2004).